

SOURCE LOCALIZATION ON SOLIDS UTILIZING TIME-FREQUENCY ANALYSIS OF PARAMETERIZED WARPED SIGNALS

Arun R. Kattukandy, Vaninirappuputhenpurayil Gopalan Reju and Andy W. H. Khong

Department of Electrical and Electronic Engineering
Nanyang Technological University, Singapore
Email: arun4@e.ntu.edu.sg, {reju, andykhong}@ntu.edu.sg.

ABSTRACT

We propose a new approach for source localization on solids with applications to human-computer interface. We analyze the wave propagation of flexural modes of vibration, generated by an impact on a solid surface, to characterize the dispersive linear time-varying system having non-linear phase response. We show that a difference in dispersion between two signals propagating through solids can be mapped directly to the relative propagation distance if the signals are appropriately time-warped. We then exploit this important property for source localization by computing the similarity of the warped signals in the time-frequency domain. As the proposed source localization algorithm jointly estimates warping-based polynomial parameters and source location, the method does not require pre-calibration.

Index Terms— Human-computer interaction, frequency dispersion, source localization on solids, unitary warping.

1. INTRODUCTION

Source localization using signals propagating on a solid surface has attracted much interest over the years for applications such as fracture analysis in structures using acoustic emission [1]. More recently, this area of research has found application in the conversion of rigid flat surfaces (such as tabletops and glass panels) into touch interfaces [2] [3] [4] [5]. For such human-computer interface applications, source localization algorithms have been developed to localize the point of impact due to touch using signals acquired by surface-mounted vibration sensors. While the use of time-differences-of-arrival (TDOA) techniques have been proposed in [6] [7], these techniques may not be well-suited since the dispersive nature of wave propagation on solids introduce non-linear time-frequency distortion [8]. Analysis of the received signals still remains a challenge due to temperature variation [9], different modes of wave propagation as well as wave distortion caused by dispersive nature of the channels between the tap impact location and the sensors. To achieve a reasonably good accuracy, TDOA based algorithms generally require a priori knowledge of material properties which are normally obtained during calibration [1] [10] [11].

Passive source localization techniques such as the time-frequency Hermitian angle (TiF-HA) approach [12] and Kullback-Leibler discrimination information (KLID) [13] have shown to achieve promising localization accuracy without prior knowledge of material properties. These algorithms achieve source localization via

time-of-arrival (TOA) estimation by exploiting the spectral diversity of a signal before and after the onset point. The KLID algorithm estimates the phase transit time by maximizing the Kullback-Leibler distance between the periodogram of neighboring signal frames. In the case of TiF-HA, an analysis vector is formed by concatenating a complex element (taken from a uniformly distributed random variable) with a signal element in the time-frequency domain. The TOA is then estimated by finding the crossover point where the standard deviation of the Hermitian angles between the analyzing vector and a randomly selected reference vector (calculated across frequency bins) exceeds a pre-determined threshold. Since TOA-based methods estimate the source location by assuming a single onset point within each received signal, localization accuracy is sensitive to additive noise. It is important to note that, unlike conventional TDOA based methods such as generalized cross-correlation (GCC) [14] which exploit the coherence between the received signals, the above TDOA-based source localization methods are not robust against uncorrelated sensor and/or thermal noise. In addition, existing methods such as those presented in [12] [13] require calibration for the estimation of phase velocities. This, in turn, may cause inconvenience to potential users.

Unlike in [12] and [13], we estimate the range difference between pairs of source-sensor in order to avoid the need of velocity estimation. To achieve this, we analyze wave propagation through solids and show that any dispersion in solids can be represented by a non-linear change in phase function. Therefore, a difference in dispersion can be mapped directly to a difference in relative propagation distances if the signals are properly time-warped. This property is then exploited for source localization by quantifying the similarity of the warped signal in the time-frequency domain. As the proposed source localization algorithm jointly estimates warping based polynomial parameters and source location, it does not require pre-calibration.

2. PROPOSED ALGORITHM

We consider waves propagating on thin rectangular plate surfaces. We gain insights into the dispersive behavior of the signal propagation (due to non-linear phase function) from the solution of the wave equation. These non-linearities can be linearized by an appropriate time-frequency resampling warping function, which is dependent on material properties. To avoid material-based calibration, we generalize the warping by approximating the solution using a parametrized warping function.

This work was supported by Ministry of Education, Singapore under research grant MOE2012-TIF-1-T-049, in partnership with the Institute of Technical Education, Singapore.

2.1. Flexural Vibration of Thin Plate

We consider, at time t , the vertical displacement $q_i(x_i, y_i, t)$ of the plate surface for the i th sensor at location (x_i, y_i, t) due to a force function $P(x', y', t)$ at location (x', y') . According to the wave propagation model [15]

$$P(x', y', t) = D\nabla_i^4 q_i(x_i, y_i, t) + \mu \frac{dq_i(x_i, y_i, t)}{dt} + \rho L_z \frac{d^2 q_i(x_i, y_i, t)}{dt^2}, \quad (1)$$

where μ is the absorption coefficient of the plate material, ρ the density, L_z the thickness of the plate, D is the stiffness of the plate and ∇_i^4 represents the biharmonic operator evaluated at (x_i, y_i) such that $\nabla^4 = \frac{\partial^4}{\partial x^4} + 2\frac{\partial^4}{\partial x^2 \partial y^2} + \frac{\partial^4}{\partial y^4}$. To solve (1), we express $P(x', y', t)$ due to an impact at (x', y') as $P(x', y', t) = p(t)\delta(x-x')\delta(y-y')$, where $p(t)$ is any arbitrary function in time and $\delta(x)$, $\delta(y)$ are the Dirac delta functions with respect to spatial variables x and y , respectively. The approximate solution for (1) in the space-frequency domain for an angular frequency ω is given by [16]

$$\underline{q}_i(r_i, \omega) = \underline{P}(\omega)e^{-jk(\omega)r_i}, \quad (2)$$

where $\underline{P}(\omega)$ is the far-field solution of bending wave equation and $r_i = \sqrt{(x_i - x')^2 + (y_i - y')^2}$ is the distance between the point of impact and the i th sensor. The wavenumber $k(\omega)$ can be obtained from the homogeneous solution of (1) as

$$k(\omega) = \sqrt[4]{(\rho L_z)/D}\sqrt{\omega}. \quad (3)$$

The phase velocity, which defines the rate of propagation of particles corresponding to a single angular frequency ω , is then given by

$$c_p(\omega) = \omega/k(\omega) = \sqrt[4]{D/(\rho L_z)}\sqrt{\omega} \quad (4)$$

while the group velocity

$$c_g(\omega) = d\omega/dk(\omega) = 2c_p(\omega) \quad (5)$$

defines the rate of propagation of the signal energy. The difference between $c_p(\omega)$ and $c_g(\omega)$ results in (inter-modal) dispersion of the wave. This dispersive behavior of (3) results in a non-linear variation in phase of (2) with respect to ω .

Any dispersive linear time-varying systems can be characterized by the non-linear phase function of the signal with respect to time [17] [18]. These non-linear functions are specific to the nature of the channel through which the signal propagates. Such transformations can be modeled using warping-based time-frequency resampling of the original signals [19].

2.2. Time-frequency Warping

The warping transform is a time-frequency resampling transformation which transforms the time-domain variable $q_i(t)$ into a warped version $\tilde{q}_i(t)$ using a unitary mapping function. This mapping can either be performed in time domain using $\xi(t)$, or in frequency domain using $\underline{\xi}(\omega)$. Therefore the warped version of $q_i(t)$ is given by

$$\tilde{q}_i(t) = \sqrt{|d\xi(t)/dt|}q_i[\xi(t)], \quad (6)$$

where operation $q_i[\xi(t)]$ implies sampling $q_i(t)$ according to the warping function $\xi(t)$. The functional inverse of $\xi(t)$ can then be

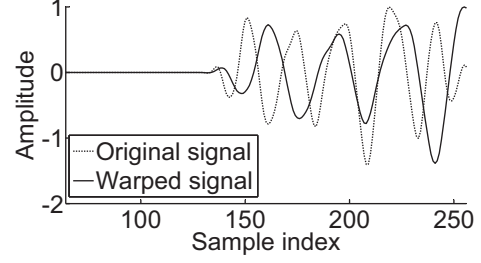


Fig. 1. Effect of warping the signal in time domain (after time aligning both signals), where $\kappa = 300f_s^{-1}$.

defined as $\xi^{-1}(t)$ such that $\xi^{-1}[\xi(t)] = t$. The corresponding mapping function $\underline{\xi}(\omega)$ which maps the change in sampling of frequency axis due to $\xi(t)$ is given by

$$\underline{\xi}(\omega) = \omega\sqrt{|d\xi^{-1}(t)/dt|}. \quad (7)$$

Similarly, the functional inverse of $\underline{\xi}(\omega)$ can be defined as $\underline{\xi}^{-1}(\omega)$ such that $\underline{\xi}^{-1}[\underline{\xi}(\omega)] = \omega$. Noting that $\tilde{q}_i(t)$ and $q_i(t)$ have the same energy, the warping function satisfies unitary equivalence.

We now consider the case where $\underline{\xi}^{-1}(\omega) = k(\omega)$. Applying the warping operator to (2) yields signal $\tilde{q}_i(t)$ in space-frequency domain given by

$$\tilde{q}_i(r_i, \omega) = \underline{P}[\underline{\xi}(\omega)]\sqrt{|d\underline{\xi}^{-1}(\omega)/d\omega|}e^{-j\omega r_i} \quad (8)$$

in which the non-linear change in phase of $q_i(r_i, \omega)$ is transformed to a linear function in warped domain $\tilde{q}_i(r_i, \omega)$. Now, for a signal propagated by a distance of $r_i + \Delta r$,

$$\tilde{q}_i(r_i + \Delta r, \omega) = \tilde{q}_i(r_i, \omega)e^{-j\omega\Delta r}. \quad (9)$$

We therefore note that proper selection of $\xi(t)$ will translate the change in dispersion due to $k(\omega)$ to a linear function of range difference. The accuracy of this characterization is highly dependent on the priori information of $k(\omega)$. As described in [20] [21], $k(\omega)$ may be available or can be derived based on physical dimensions and mechanical properties of the medium. Such pre-calibration imposes strong assumptions on the material properties and any variation in $k(\omega)$ due to, for example, caused by a change in environment [9], will degrade the localization performance.

2.3. Parametrized Time Warping

We address the above problem by jointly estimating the warping-related polynomial parameters and source location. With reference to Section 2.2, (9) also indicates that the range difference between two propagation paths can be estimated from the change in dispersion between the two signals. We therefore propose to utilize time-frequency representations of the parametrized warped signals.

Unlike (8) which requires material properties, we propose to approximate the wave propagation in plates with that of normal mode propagation in an ideal waveguide. In an ideal waveguide, the propagation of particles in time domain, for mode l with an angular frequency of ω_l , is given by [19] [22]

$$q_i^l(t) = |q_i^l(t)|e^{j\omega_l\sqrt{t^2 - \kappa^2}}, \quad (10)$$

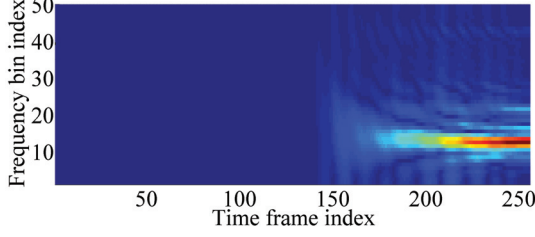


Fig. 2. Spectrogram of a sensor output due to a metal stylus tap on an aluminum plate surface.

where $|q_i^l(t)|$ is the instantaneous amplitude of mode l and κ is the unknown propagation delay in a non-dispersive environment. Therefore the time-domain warping function parametrized by κ to satisfy phase linearity is given by [23]

$$\xi_\kappa(t) = \sqrt{t^2 + \kappa^2}, \quad (11)$$

and in an ideal waveguide, the time warped signal will be

$$\hat{q}_i^l(t) = \sqrt{|d\xi_\kappa(t)/dt|} |q_i^l[\xi_\kappa(t)]| e^{j\omega t}. \quad (12)$$

From (12), for each warped mode, the instantaneous phase ωt is now linear in time. Here κ is used to parametrize the dispersion or spreading of the signal as illustrated in Fig. 1, for the case of $\kappa = 300f_s^{-1}$, where f_s is the sampling frequency.

In the context of our application, assuming $w_i(t)$ and $w_j(t)$ are the two sensor outputs induced by the vertical displacement $q_i(t)$ and $q_j(t)$ respectively, our objective is to find an optimal warping parameter κ^{opt} such that

$$w_i(t) \approx \sqrt{|d\xi_\kappa^{\text{opt}}(t)/dt|} |w_j[\xi_\kappa^{\text{opt}}(t)]| e^{j\omega t}, \quad (13)$$

where

$$\xi_\kappa^{\text{opt}}(t) = \sqrt{t^2 + (\kappa^{\text{opt}})^2}. \quad (14)$$

To estimate κ^{opt} , we warp one of the two sensor signals over a range of κ and each warped signal will be checked for similarity with the other signal by analyzing them in the time-frequency domain. The value of κ giving the maximum similarity will then be taken as κ^{opt} .

To describe the above, we define $\tilde{w}_j^\kappa(n)$ as the time-warped version of $w_j(n)$ computed via (11) and (6) using a value of κ . We next transform both $w_i(n)$ and $\tilde{w}_j^\kappa(n)$ into the time-frequency domain using short-time Fourier transform (STFT) so that $\underline{w}_i(b, m)$ and $\underline{\tilde{w}}_j^\kappa(b, m)$ are the STFT coefficients of $w_i(n)$ and $\tilde{w}_j^\kappa(n)$, respectively, where b is the frequency bin index and m is the time frame index. Since the algorithm is insensitive to spectral leakage across frequency bins, in order to save computational cost and to avoid amplitude smoothing around the onset point, we have used the rectangular window for the STFT analysis. To preserve maximum time resolution, the hop size is fixed as one sample.

Due to the trade-off between high frequency resolution and computational complexity, we have chosen the maximum number of frequency bins to be 256. Figure 2 shows the spectrogram of a sensor output due to a stylus tap on an aluminum plate. We note that beyond frequency bin $b > 30$ (corresponding to a frequency of 11 kHz), the energy of the signal is negligibly small. This is consistent with the frequency response of the Murata PKS1-4A10 used in our experiment. Hence, in order to reduce the computational cost and influence of noise, we have limited the analysis of frequency bins to $10 \leq b \leq 20$.

Here the warped signals $\tilde{w}_j^\kappa(n)$ are estimated by resampling the samples of $w_j(n)$ at $\xi_\kappa(t)$ using linear interpolation. Interpolation is required since most of the samples are lying in the non-integer multiple of the sampling frequency $f_s = 96$ kHz. In our analysis we iterate the signal similarity analysis over $0 \leq \kappa \leq 100 \times 2f_s^{-1}$.

The estimate of the optimal warping operator κ^{opt} is then obtained as

$$\hat{\kappa}^{\text{opt}} = \arg \min_{\kappa} \mathcal{J}(\kappa), \quad (15)$$

where $\mathcal{J}(\kappa)$ quantifies the similarity between a received signal and the warped signal of the other channel given by

$$\mathcal{J}(\kappa) = \sum_{b=b_{\min}}^{b_{\max}} \frac{(\underline{w}_i(b) - \underline{\tilde{w}}_j^\kappa(b)) (\underline{w}_i(b) - \underline{\tilde{w}}_j^\kappa(b))^T}{M(b_{\max} - b_{\min} + 1)}, \quad (16)$$

given that $\underline{w}_i(b)$ and $\underline{\tilde{w}}_j^\kappa(b)$ is the frequency bin-wise normalized version of $\underline{w}_i(b, m)$ and $\underline{\tilde{w}}_j^\kappa(b, m)$, respectively, in decibel (dB) across $m = 0, 1, \dots, M - 1$, M is the total number of time frames, and b_{\min} and b_{\max} are, respectively, the lower and upper range of the frequency bins.

Since $w_i(n)$ and $\tilde{w}_j^\kappa(n)$ are defined for $t \geq 0$, (11) is valid only for $t > \kappa$. This implies that the sensor nearest to the point of impact is chosen as the reference sensor to avoid negative range difference. This reference sensor can be identified using one of the onset detection algorithms such as presented in [12] [13].

2.4. Source Position Estimation

To estimate the source location, we propose a polynomial relation model between differences in the source-sensor range and the optimal warping parameter. Utilizing this model, we estimate the source position by minimization of a non-linear cost function.

Establishing the relationship between the range differences and the optimal warping parameters can be achieved by taping at known locations on an aluminum plate surface using a metal stylus. Since the tap/source locations are known, the range differences is also known and these points are plotted against the corresponding optimal warping parameters as shown in Fig. 3 as dotted points. In this plot, $\hat{\kappa}_{\gamma,i}^{\text{opt}}$ represents the estimated optimal warping parameter corresponding to the range difference $r_{\gamma,i}$ between the nearest sensor γ and the i th sensor. A polynomial curve is then fitted on the data as shown in Fig. 3. From the experimental results conducted on different plate surfaces we found that a polynomial function of order two is sufficient to describe the relationship between the range differences and the optimal warping parameters. Hence, we propose to use a second-order polynomial function relating $r_{\gamma,i}$ and $\hat{\kappa}_{\gamma,i}^{\text{opt}}$ as follows

$$\hat{r}_{\gamma,i} = \alpha_1 (\hat{\kappa}_{\gamma,i}^{\text{opt}})^2 + \alpha_2 (\hat{\kappa}_{\gamma,i}^{\text{opt}}) + \alpha_3, \quad (17)$$

where α_1 , α_2 and α_3 are the unknown polynomial parameters which depends on the medium of wave propagation. The relative range difference $\hat{r}_{i,j}$ between Sensors i and j can now be expressed in terms of (17) as

$$\begin{aligned} \hat{r}_{i,j} &= \hat{r}_{\gamma,i} - \hat{r}_{\gamma,j} \\ &= \hat{\alpha}_1 ((\hat{\kappa}_{\gamma,i}^{\text{opt}})^2 - (\hat{\kappa}_{\gamma,j}^{\text{opt}})^2) + \hat{\alpha}_2 (\hat{\kappa}_{\gamma,i}^{\text{opt}} - \hat{\kappa}_{\gamma,j}^{\text{opt}}), \end{aligned} \quad (18)$$

where $\hat{\alpha}_1$ and $\hat{\alpha}_2$ are estimates of α_1 and α_2 . While these estimates are not required to determine source position, they are jointly estimated using optimization algorithms as will be described below.

Assuming known sensor positions and defining r_i as the distance between the source and the i th sensor, the unknown source position

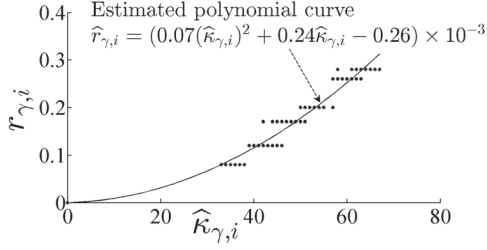


Fig. 3. Variation of optimal warping parameter $\kappa_{\gamma,i}$ with range difference $r_{\gamma,i}$.

(x', y') can be estimated by minimizing the error function

$$(\hat{x}', \hat{y}') = \arg \min_{x', y', \alpha_1, \alpha_2} \sum_{i,j} (r_i - r_j - \hat{r}_{i,j}), \quad (19)$$

where $\hat{r}_{i,j}$ is calculated from (18) and $r_i = \sqrt{(x' - x_i)^2 + (y' - y_i)^2}$. Such minimization can be performed using, for example, the iterative Levenberg-Marquardt optimization algorithm [24].

3. EXPERIMENTAL RESULTS

To quantify the performance of the algorithm in terms of accuracy, we adopt the root-mean-square error (RMSE) given by

$$\text{RMSE} = \sqrt{\frac{1}{T} \sum_{u=1}^T (x'(u) - \hat{x}'(u))^2 + (y'(u) - \hat{y}'(u))^2}, \quad (20)$$

where tap index $1 \leq u \leq T$, T is the total number of taps, and $[x'(u), y'(u)]^T$ is the actual tap position while $[\hat{x}'(u), \hat{y}'(u)]^T$ is the estimated position of the u th tap.

To verify the performance of the proposed method, experiments were conducted on aluminum and glass surfaces having dimension of $0.6 \text{ m} \times 0.6 \text{ m} \times 2.5 \text{ mm}$ and $0.6 \text{ m} \times 0.6 \text{ m} \times 5.0 \text{ mm}$, respectively. Eight Murata PKS1-4A1 shock sensors were placed 10 cm apart along the inner square perimeter of the test surfaces. Nine tap locations are arranged in a uniform grid of 3×3 array inside the area enclosed by the sensor array where the separation between the nearest row and column tap positions is 10 cm as described in [12]. The tap locations were sequentially tapped using a metal stylus and a finger. Each position is tapped five times giving $T = 45$. The received signals were digitized at $f_s = 96 \text{ kHz}$ sampling frequency with 24-bit resolution. We have used $B = 1024$ for TiF-HA and for the proposed algorithm, $B = 256$ was found to be suitable given the trade-off between computational complexity and frequency resolution. Figure 4 illustrates the variation of \mathcal{J} with respect to κ using data collected on aluminum surface, tapped with the metal stylus. It is interesting to see that \mathcal{J} is a convex function with respect to κ and this allows one to easily determine its minimum. Hence, for the cases shown in Fig. 4, $\hat{\kappa}_{\gamma,1}^{\text{opt}} = 0$, $\hat{\kappa}_{\gamma,2}^{\text{opt}} = 49$ and $\hat{\kappa}_{\gamma,3}^{\text{opt}} = 64$. As expected, value of κ^{opt} increases with range difference.

As shown in [11], TiF-HA achieves an overall improvement in localization accuracy compared to methods based on the Kullback-Leibler discrimination information [13] and wavelet [25]. Hence, in this work we compare the performance of the proposed algorithm with that of TiF-HA only. Figure 5 compares the performance of the proposed algorithm with TiF-HA in terms of RMSE and standard deviation in RMSE for source localization. The results show that, for taps made by the stylus, the proposed algorithm can achieve

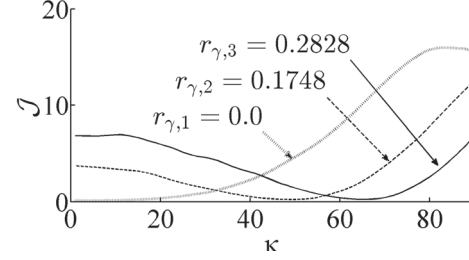


Fig. 4. Variation of \mathcal{J} with respect to κ (scaled by $2f_s^{-1}$) for various values of range difference for aluminum plate surface.

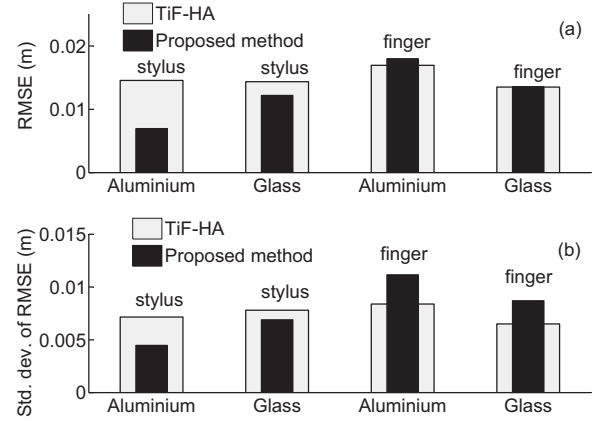


Fig. 5. Performance comparison of the proposed algorithm with TiF-HA algorithm (a) RMSE in source localization and (b) standard deviation of RMSE in source localization.

reduction in RMSE of 7 mm and 2 mm compared to TiF-HA, for aluminum and glass surfaces, respectively. The standard deviations of proposed algorithm is also lower compared to TiF-HA. For impacts made by the finger, the RMSE and standard deviation are only modestly higher than that of TiF-HA. The increase in RMSE for aluminum is about 1 mm whereas for glass it is 0.1 mm. Similarly, the standard deviation in RMSE is also modestly higher; approximately 3 mm for aluminum and 2 mm for glass, compared to that of TiF-HA. For a large surface considered in this experiment, such degradation is insignificant and in addition, unlike TiF-HA, the proposed algorithm does not require pre-calibration.

4. CONCLUSION

We propose a source localization algorithm on solids. This algorithm exploits the similarity of the warped dispersive signal in time-frequency domain. We analyzed the wave propagation of flexural vibration due to an impact on a plate surface and show that the change in dispersion between two signals is dependent on the range difference between the propagation path of the signals. Utilizing this, we developed a source localization algorithm for impact localization on solid surfaces. As the proposed source localization algorithm jointly estimates the model parameters and source location, this method does not require pre-calibration. The algorithm is validated via experiments conducted on aluminum and glass plates, for both stylus and finger taps.

5. REFERENCES

- [1] H. Jeong and Y. S. Jang, "Fracture source location in thin plates using the wavelet transform of dispersive waves," *IEEE Trans. Ultrason., Ferroelectr., Freq. Control*, vol. 47, no. 3, pp. 612–619, 2000.
- [2] D. T. Pham, M. Al-Kutubi, Z. Ji, M. Yang, Z. Wang, and S. Catheline, "Tangible acoustic interface approaches," in *Proc. Virtual Conf., IPROMs*, Ed., May 2005.
- [3] A. Sulaiman, K. Poletkin, and A. W. H. Khong, "Source localization in the presence of dispersion for next generation touch interface," *Proc. IEEE Cyberworlds*, pp. 82–86, 2010.
- [4] D. T. Pham, Z. Wang, Z. Ji, M. Yang, M. Al-Kutubi, and S. Catheline, "Acoustic pattern registration for a new type of human-computer interface," in *Virtual Conference, IPROMs*, Ed., May 2005.
- [5] X. Yap, A. W. H. Khong, and W.-S. Gan, "Localization of acoustic source on solids: A linear predictive coding based algorithm for location template matching," *Proc. IEEE Int. Conf. on Acoust. Speech and Signal Process.*, 2010.
- [6] S. M. Ziola and M. R. Gorman, "Source location in thin plates using cross-correlation," *J. Acoust. Soc. Am.*, vol. 90, pp. 2551–2556, 1991.
- [7] W. Rolshofen, D. T. Pham, M. Yang, Z. B. Wang, Z. Ji, and M. Al-Kutubi, "New approaches in computer-human interaction with tangible acoustic interfaces," in *Proc. Virtual Int. Conf., IPROMs*, Ed., May 2005.
- [8] K. R. Arun, X. Yap, and A. W. H. Khong, "A touch interface exploiting time-frequency classification using Zak transform for source localization on solids," *IEEE Trans. Multimedia*, vol. 13, no. 3, pp. 487–497, 2011.
- [9] G. Ribay, S. Catheline, D. Clorennec, R. K. Ing, N. Quieffin, and M. Fink, "Acoustic impact localization in plates: properties and stability to temperature variation," *IEEE Trans. Ultrason., Ferroelectr., Freq. Contr.*, vol. 54, pp. 378–385, 2007.
- [10] Y. T. Chan, T. K. C. Lo, and H. C. So, "Passive range-difference estimation in a dispersive medium," *IEEE Trans. Signal Process.*, vol. 58, no. 3, pp. 1433–1439, 2010.
- [11] L. De Marchi, A. Perelli, and A. Marzani, "A signal processing approach to exploit chirp excitation in lamb wave defect detection and localization procedures," *Mech. Syst. Signal Process.*, 2012.
- [12] V. G. Reju, A. W. H. Khong, and A. Sulaiman, "Localization of taps on solid surfaces for human-computer touch interfaces," *IEEE Trans. Multimedia*, vol. 15, no. 6, p. 1365, 2013.
- [13] K. R. Arun, E. Ong, and A. W. H. Khong, "Source localization on solids using Kullback-Leibler discrimination information," *Proc. IEEE Conf. Information, Communications, Signal Processing*, pp. 1–5, 2011.
- [14] C. Knapp and G. C. Carter, "The generalized correlation method for estimation of time delay," *IEEE Trans. Acoust., Speech, Signal Process.*, vol. 24, no. 4, pp. 320–327, 1976.
- [15] E. Ventsel and T. Krauthammer, *Thin plates and shells: theory, analysis, and applications*. Marcel Dekker, Inc., 2001.
- [16] A. Berkhout, D. de Vries, and M. C. Brink, "Array technology for bending wave field analysis in constructions," *J. Sound Vib.*, vol. 300, no. 1-2, pp. 25 – 42, 2007.
- [17] A. Papandreou-Suppappola, R. L. Murray, B. Iem, and G. F. Boudreaux-Bartels, "Group delay shift covariant quadratic time-frequency representations," *IEEE Trans. Signal Process.*, vol. 49, no. 11, pp. 2549–2564, 2001.
- [18] C. Ioana, J. I. Mars, A. Serbanescu, and S. Stankovic, "Time-frequency-phase tracking approach: Application to underwater signals in a passive context," *Proc. IEEE Int. Conf. on Acoust. Speech and Signal Process.*, pp. 5634–5637, 2010.
- [19] Y. Jiang and A. Papandreou-Suppappola, "Discrete time-frequency characterizations of dispersive linear time-varying systems," *IEEE Trans. Signal Process.*, vol. 55, no. 5, pp. 2066–2076, 2007.
- [20] I. Bartoli, A. Marzani, F. L. di Scalea, and E. Viola, "Modeling wave propagation in damped waveguides of arbitrary cross-section," *J. Sound Vib.*, vol. 295, no. 35, pp. 685 – 707, 2006.
- [21] A. Roueff, J. Mars, J. Chanussot, and H. Pedersen, "Dispersion estimation from linear array data in the time-frequency plane," *IEEE Trans. Signal Process.*, vol. 53, no. 10, pp. 3738–3748, 2005.
- [22] C. Ioana, A. Jarrot, C. Gervaise, Y. Stéphan, and A. Quinquis, "Localization in underwater dispersive channels using the time-frequency-phase continuity of signals," *IEEE Trans. Signal Process.*, vol. 58, no. 8, pp. 4093–4107, 2010.
- [23] J. Bonnel, B. Nicolas, J. I. Mars, and S. C. Walker, "Estimation of modal group velocities with a single receiver for geoacoustic inversion in shallow water," *J. Acoust. Soc. Am.*, vol. 128, no. 2, pp. 719–727, 2010.
- [24] D. W. Marquardt, "An algorithm for least-squares estimation of nonlinear parameters," *J. Soc. Ind. Appl. Math.*, vol. 11, no. 2, pp. 431–441, 1963.
- [25] L. Gaul and S. Hurlebaus, "Identification of the impact location on a plate using wavelets," *Mech. Syst. Signal Process.*, vol. 12, no. 6, pp. 783 – 795, 1998.